PCCP

Sub-Surface Alloying Largely Influences Graphene Nucleation and Growth over Transition Metal Substrates

Journal:	*Physical Chemistry Chemical Physics*
Manuscript ID:	CP-ART-07-2015-003820.R1
Article Type:	Paper
Date Submitted by the Author:	27-Jul-2015

Complete List of Authors:	Zhang, Liying; Zhengzhou University, School of Physcis and Engineering Zhao, Xingju; Zhengzhou University, School of Physcis and Engineering Xue, Xinlian; Zhengzhou University, School of Physcis and Engineering Shi, Jinlei; Zhengzhou University, School of Physcis and Engineering Ren, Xiaoyan; Zhengzhou University, School of Physcis and Engineering niu, chunyao; Zhengzhou University, School of Physcis and Engineering Li, Chong; Zhengzhou University, School of Physics and Engineering Jia, Yu; Zhengzhou University, School of Physcis and Engineering Guo, Zhengxiao; University College London, Department of Chemistry Li, Shunfang; Zhengzhou University, School of Physcis and Engineering

Sub-Surface Alloying Largely Influences Graphene Nucleation and Growth over Transition Metal Substrates

Liying Zhang[1], Xingju Zhao[1], Xinlian Xue[1], Jinlei Shi[1], Chong Li[1], Xiaoyan Ren[1], Chunyao Niu[1], Yu Jia[1], Zhengxiao Guo[2, 1*], and Shunfang Li[1†]

[1]International Laboratory for Quantum Functional Materials of Henan, School of Physics and Engineering, Zhengzhou University, Zhengzhou, 450001, China

[2]Department of Chemistry, University College London, London WC1H 0AJ, UK

Abstract

Sub-surface alloying (SSA) can be an effective approach to tuning surface functionalities. Focusing on Rh(111) as a typical substrate for graphene nucleation, we show strong modulation by SSA atoms to both the energetics and kinetics of graphene nucleation simulated by first-principles calculations. Counter-intuitively, when the sub-surface atoms are replaced by more active solute metal elements to the left of Rh in the Periodic Table, such as earlier transition metals (TMs), Ru and Tc, the binding between a C atom and the substrate is weakened and two C atoms favor dimerization. Alternatively, when the alloying elements are later TMs to the right of Rh, such as relatively inert Pd and Ag, the repulsion between the two C atoms are enhanced. Such distinct results can be well addressed by the delicately modulated activities of the surface host atoms in the framework of the *d*-band theory. More specifically, we establish a very simple selection rule in optimizing the metal substrate for high quality graphene growth: the introduction of an earlier (later) solute TM in the SSA lowers (raises) the *d*-band center and the activity of the top-most host metal atoms, weakening (strengthening) the C-substrate binding, meanwhile both energetically and kinetically facilitating (hindering) the graphene nucleation, and simultaneously promoting (suppressing) the orientation disordering the graphene domains. Importantly, our preliminary theoretical results show also that such a simple rule is also proposed to be operative for graphene growth on the widely invoked Cu(111) catalytic substrate.

1. Introduction

Graphene[1] is a single atomic layer of hexagonally packed carbon atoms, and the basic building block of graphitic materials of all other dimensionalities.[2] As a striking star material, it has attracted considerable attention due to its remarkable electrical,[2, 3] mechanical[2, 4] and chemical properties[5] for potential applications in electronics,[2] optoelectronics,[6] thermal transport,[7] catalysis,[8, 9] lithium-ion batteries,[10] and chemical and biological sensing.[11] Underpinning all the cases is the primary challenge for cost-efficient, reliable, and high-throughput synthesis of a high-quality single-crystal monolayer graphene. Correspondingly, various methods for synthesizing large-area graphene monolayers have been investigated, such as graphitization of silicon carbide surfaces[12, 13] and catalytic chemical vapor deposition (CVD) of carbon sources on transition metals (TMs), such as Ru,[14, 15] Rh,[16] Ir,[17, 18] Ni,[19, 20] Pt,[21, 22] Pd,[23] and Cu.[24-27] Among these different avenues, CVD stands out in stark contrast to others as a highly promising technique of synthesizing large-scale high-quality monolayer graphene, which can be readily transferred to other substrates via chemical etching. However, up to date, the mass production of graphene mainly results in polycrystalline structures, consisting of undesirable grain boundaries (GBs) that may degrade their functionalities in practice.

Extensive efforts have been devoted to explore the underlying mechanisms of graphene nucleation, growth and the formation of grain boundaries on various TM substrates in the context of CVD synthesis. For example, carbon supersaturation was revealed to play an important role in graphene growth on Ir(111)[18] and Ru(0001)[28] substrates, and a carbon-cluster attachment mechanism[29-31] has been proposed for such systems. On a Cu substrate,[24-27, 32] surface adsorption process dominates the graphene growth, whereas on Ni[19, 20] carbon segregation is the main

mechanism. Furthermore, the initial nucleation stages of carbon adatoms on TM substrates are widely investigated. Experimentally, it has been revealed that carbon nucleation prefers to start from the step edges over terraces on Ir(111),[18] Ru(0001),[28] and Ni(111)[19, 20] surfaces; theoretically, Chen *et al*.[32] have elucidated that the delicate competition between the C-C and C-metal interactions on the step edges and/or terraces of the TM substrate essentially determines the initial nucleation of graphene epitaxial growth. More specifically, the binding of carbon adatoms, dimer or carbon clusters with the step edges/terraces of TM substrate also ultimately determines the features of grain boundaries. Briefly, a relatively weak C-metal coupling with respect to C-C interaction enables fast diffusion of carbon atoms and results in multi-site nucleation of carbon islands over the whole surface, and leads to grain boundaries when different graphene grains coalesce together at different orientations, as reported for graphene growth on Cu.[24-27, 33] Alternatively, GBs can also be formed in the initial nucleation stage when several graphene grains emanate from one nucleation site.[34] Somewhat intuitively, C dimerization is not preferred on a TM terrace with relatively strong C-TM binding, interestingly, the carbon nucleation is readily facilitated by the step edges due to the geometric effect.[32] However, it is more desirable for nucleation of graphene islands to take place over the entire substrate rather than merely at the preexisting step edges. Since the specific interactions of the C seeds with the catalytic surface is critical in determining the quality of the produced graphene, consequently, some efforts have been devoted to suppressing the prevalence of grain boundaries by selecting highly appropriate substrates. For example, surface alloy Mn-Cu(111)[33, 35, 36] superstructure was invoked to suppress the grain orientation disordering; and more recently, Wafer-scale single-crystal graphene with predefined orientation was fabricated with the aid of anisotropic twofold symmetry of a

hydrogen-terminated Ge(110) surface.[37]

Motivated by such efforts in fabricating high-quality and large-scale single-crystal graphene, in this paper, we propose another new approach - using sub-surface alloy (SSA) effect[38] to modulate the delicate C-metal coupling and the C-C interaction, which essentially determines both the energetics and kinetics of carbon nucleation at the initial stages of graphene epitaxial growth on metal surfaces. The central purpose here is to establish the design principles in fabricating appropriate metal substrate for optimizing graphene nucleation and suppressing the orientation disordering of the graphene domains over the entire flat terraces of the SSA. Specifically, in the SSAs, a series of different TMs have been sandwiched between the first and second layer of a host metal substrate, therefore the topmost layer of the SSA substrate consists of mainly one type of the host metal atoms, rather than forming a rigorous surface superstructure.[33, 35, 36] Additionally, the SSA metal substrates are expected to possess significantly higher catalytic activities than the hydrogen-terminated Ge(110) surface,[37] which is critical for graphene growth at low temperatures via the CVD method. Such sub-surface alloys[38] have been extensively studied as oxygen reduction catalysts in fuel cells.[39, 40] However, the validity of the SSA in optimizing graphene growth has not been examined before. Taking Rh(111) as a prototypical example, we find that on Rh(111) two C atoms prefer separation, counter-intuitively, when the sub-surface atoms are replaced by solute metal elements to the left of Rh in the Periodic Table, such as earlier transition metal Ru and Tc with a higher *d*-band center, the two C atoms tend to form a dimer. On the other hand, when the solute metal components are the later TMs, such as relatively more inert Pd and Ag elements of lower *d*-band centers,[41, 42] the repulsion between the two C atoms are enhanced, hindering the nucleation of graphene. Additionally, such an SSA effect also significantly modulates the

stabilities of larger C clusters on the metal surface. Importantly, the earlier (later) solute atoms in the SSA facilitate (hinder) the C diffusion on the surface, while the later solute TMs can effectively suppress the orientation disordering of the graphene domains on the SSA substrates, as also demonstrated by our preliminary calculations on the graphene growth on the widely used Cu(111)[24, 32] catalytic substrate.

2. Methods

Our density functional theory (DFT) calculations are carried out using the Vienna ab initio simulation package (VASP)[43] with PAW potentials[44, 45] and the generalized gradient approximation (PBE-GGA)[46] for the exchange-correlation functional. In our calculations, we first take Rh(111) as a prototypical host substrate and then construct some SSA systems. The lattice constants of all the TM crystals are obtained via structural optimizations. The substrate of the sub-surface metal alloy is modeled by a three- or four- layered slab, wherein a solute metal is present in the second layer of the surface. The vacuum layers are more than 13 Å thick to ensure decoupling between neighboring slabs. As detailed later in the results section, 3-layered slab is already thick enough to describe the sub-surface alloy effect in modulating the preference of carbon nucleation or not on metal substrates. During relaxation, all atoms of the slab are allowed to relax until the forces on them are smaller than 0.01 eV/Å within the spin polarized calculations. In simulating small C_N clusters ($N \leq 5$) nucleation on the metal alloy, a 4×4×1 k-point mesh was used for the 3×3 surface unit cell; for the cases of C_N clusters ($N > 5$), a 3×2×1 k-point sampling for the 4×8 surface unit cell was adopted.[47] The energy cutoff is 400 eV in all the calculations, together with the K-point sampling, these parameters have been carefully examined to insure good convergence. The formation energy (E_f) per carbon atom on the metal substrate is calculated by the formula:

$$E_f=(N\times E_{C(atom)}+E_{substrate}-E_{adsorbate\text{-}substrate})/N \quad (1)$$

where $E_{C(atom)}$, $E_{substrate}$, and $E_{adsorbate\text{-}substrate}$ are the total energies of a free standing C atom, the metal substrate, and the optimized adsorbate-substrate complex, respectively. We use the climbing image nudged elastic band method[48] to determine the energy barriers of the various kinetic processes.

Here, we note that the criterion in selecting the solute atoms of the sub-surface is mainly based on the consideration of well-matched surface lattice constants between the solute metal and the host substrate. The calculated mismatches between the calculated surface lattices of Tc(0001), Ru(0001), and Pd(111) with Rh(111) are negligible, *i.e.*, 1.7%, 0.2%, and 2.9%, respectively. Even in the case of Ag(111), the mismatches slightly raise to 8.4%, enabling us to neglect the surface strain effect due to the alloy in the SSA and merely focus on the electronic origin of the SSA.

3. Results and Discussion

We first examine the adsorption of C monomers and the nucleation of these C seeds on the surface of a flat Rh(111) substrate simulated by a three-layered slab model.[49] Here, we consider the fcc hollow (with an atom directly below in the third layer), hcp hollow (with an atom directly below in the second layer), and the surface bridge sites for the adsorption of C atoms on a given system. The most stable adsorption site is hcp, resulting in an E_f of 7.412 eV. The fcc adsorption site is 0.327 eV less stable, and the bridge is an unstable adsorption site, in line with previous calculations on the C monomer on both Ir(111) and Ru(0001).[29, 30, 32] We then investigate the initial stages of graphene nucleation on a flat Rh(111) substrate by studying the energetics of carbon dimerization. As shown in Figs. 1(c) and 1(d), we study the interactions of two C atoms on Rh(111) with two distinct configurations: 1) the formation of a carbon dimer with one C atom

occupying the preferred hcp site and another C atom locating in the vicinity of the nearest fcc site, see Fig. 1(c), in this case the optimized C-C bond length is 1.38 Å; 2) both C atoms locate on the hcp hollow sites and possess largest separation distance in the 3×3 surface cell, Fig. 1(d). Our calculations show that the former case, *i.e.*, carbon dimerization, is energetically less stable than the latter case of C atoms separation: $\Delta E=E_{C\text{-}dimerization}-E_{C\text{-}separation}=0.426$ eV. These results indicate that on the flat Rh(111) surface the C adatoms are mutually repulsive, hindering graphene nucleation therein. Note that we have also performed calculations with a four-layered slab model, which shows a slight variation in ΔE of 0.454 eV; however, the preference of C-C separation remains the case.

We next explore the SSA effect in modulating the possibility of C-nucleation on TM metal substrates by means of the delicate competition between C-C and C-metal interactions tuned by the SSA. Again, we first perform the calculations with a three-layered slab model, and the introduced solute atoms are presented in the sub-surface, as shown in Fig. 1(a). Here, we examine the SSA effect induced by the introduction of solute elements of Pd and Ag, which are to the right side of Rh and possess fully filled *d* orbitals thus relatively low chemical activities, as compared with Rh. Intuitively, the introduction of relatively inert solute atoms Pd and Ag would significantly decrease the activities of the substrate and thus weaken the C-substrate interactions, definitely facilitating the C-dimerization and graphene nucleation. Surprisingly, we find that the C-dimerization becomes energetically even unfavorable upon the introduction of solute Pd and Ag atoms, as manifested by the even larger positive values of ΔE, 0.648 and 0.691 eV, respectively, Fig. 1(e). In view of this unfavorable effects, it is natural to search for an appropriate element on the left side of Rh, taking Ru and Tc as preliminary candidates. Somewhat counter-intuitively, the

introduction of these two more reactive solute elements in the SSA effectively facilitates carbon dimerization on the host Rh(111) substrate. For the case of Ru, *i.e.* on Ru@Rh(111), ΔE is reduced to only 0.156 eV. Particularly, on the Tc@Rh(111) substrate, ΔE becomes negative, indicating that graphene nucleation is energetically favored on the flat Tc@Rh(111) terrace. From the data presented in Fig. 1(e), we can preliminarily conclude that the introduction of an relatively earlier TM solute element (with a relatively higher *d*-band center) in the SSA can reduce the chemical activity of the substrate and thus reduce the C-substrate interaction and simultaneously enhance the C-C binding, ultimately facilitating graphene nucleation.

Once again, we also identify the observation by further calculations based on a four-layered slab model, see Fig. 1(b). Interestingly, for the cases of Pd@Rh(111) and Ag@Rh(111), the calculated values of ΔE in the four-layered slab model only change slightly, to 0.627 and 0.722 eV, from 0.648 and 0.691 eV in the three-layered slab model, respectively. These findings indicate that the preference of C-C separation on TM@Rh(111) is insensitive to the thickness of the substrate in the atomic-thick regime. On the other hand, when the solute TMs are further to the left of Rh, *i.e.*, on four-layered Ru@Rh(111) and Tc@Rh(111) substrates, the calculated ΔE varies significantly to 0.420 and 0.173 eV, from the values of 0.156 and -0.233 eV obtained with a three-layered slab model. The underlying mechanism in such a contrast thickness-dependent results for different TM@Rh(111) is still unclear. Even so, the fact that the earlier TM solute atoms in the SSA substrate facilitate the C-dimerization or graphene nucleation is firmly established. Note that, recently, high quality atomic-thick (including sing-atom-layered) sheets of Rh(111) have been elaborately fabricated,[50] and by controlling the growth conditions different core-shell nanoalloy clusters can also be synthesized.[51] It is likely that the combination of these elaborate experimental

technologies can lead to high quality TM@Rh(111) SSA thin film substrates with different atomic thicknesses, which may be utilized to further modulate graphene nucleation via the observed thickness effect.

The dimerization and graphene nucleation are also crucially determined by the kinetic processes of the adsorbed carbon seeds, therefore we now show that the diffusion barrier of the C adatoms on the flat Rh(111) substrate can also be tuned via the SSA effect. In the following section, unless otherwise stated, the calculations are performed with a three-layered model, see Fig. 1(a). The calculated surface diffusion barrier (E_{barr}) of a C monomer between a metastable fcc site and the nearest stable hcp site is 0.417 eV, which is also effectively modulated by the SSA effect, as shown in Fig. 2. On Pd@Rh(111) and Ag@Rh(111) substrates, the values of the E_{barr} are tuned up to 0.638 and 0.695 eV, respectively. Whereas, for the solute atoms to the left of Rh, *i.e.* on Ru@Rh(111) and Tc@Rh(111), the E_{barr} are lowered to 0.205 and 0.116 eV, respectively. Interestingly, the trend that the earlier (*later*) TM solute atoms reduce (*increase*) the E_{barr} of C diffusion on the surface of Rh(111) substrate is also highly correlated with the fact that the earlier (*later*) TM solute atoms facilitate (*hinder*) the C-dimerization or graphene nucleation, from the energetic point of view. On the one hand, the trend revealed here exhibits the strong predictive power in potential/practical applications of the SSA to tune graphene nucleation on a TM substrate via CVD method. On the other hand, these results invite a more fundamental analysis of the underlying physics for the SSA effect.

The classic *d*-band model can be invoked to access the underlying mechanism in dominating such a rather counter-intuitive picture of the distinct SSA effect involving different solute TM atoms. According to the *d*-band theory, the activity of a TM substrate can be correlated with the

position of its *d*-band center (E_d) in the energy spectrum,[41, 42] *i.e.*, the closer E_d of the metal substrate to the Fermi energy (E_F), the stronger the binding between the adsorbate and the TM substrate. Particularly, the activities of the topmost low-coordinated surface atoms to which that the adsorbate directly binds essentially dominate the strength of the adsorbate-substrate interactions. Therefore, in Fig. 3, we plot the calculated positions of the E_d of the top-most Rh atoms in the three-layered slabs for both pure Rh(111) substrate and TM@Rh(111) alloy structures. Here, E_d is defined as: $E_d = \frac{\int_{-\infty}^{\infty} \mathrm{PDOS}_d(E) \times (E - E_F) dE}{\int_{-\infty}^{\infty} \mathrm{PDOS}_d(E) dE}$, where the PDOS_d is the DOS projected to the *d* orbitals of the Rh atoms. As marked in the bracket, the E_d of the topmost Rh atoms in pure Rh(111) substrate is -1.677 eV, and the introduction of the left-side solute atoms, such as Ru and Tc, leads to lower E_d values of -1.797 and -1.930 eV, respectively; however, for the cases of Pd@Rh(111) and Ag@Rh(111), E_d are lifted up to -1.389 and -1.242 eV, respectively, see the red bars in Fig. 3. These results presented in Figs. 1 and 2 are thus well rationalized within the classic *d*-band model[41, 42]: the left (*right*) side solute elements introduced in the host Rh shift down (*up*) the *d*-band center of the surface Rh atom and therefore reduce (*enhance*) the binding of C-Rh, ultimately facilitating (hindering) the C dimerization and the consequent graphene nucleation.

We now discuss in more detail the underlying mechanisms of the contrast solute atoms effect in modulating the E_d of the surface Rh atoms. To do this, first, we calculate the E_d of the topmost surface atoms of the pure TM substrates (Tc(0001), Ru(0001), Rh(111), Pd(111), and Ag(111)) also with a three-layered slab model. As shown in Fig. 3, the calculated values of the E_d for the five cases almost monotonously (except for the case of Pd) drop down from the left side element Tc (-1.422 eV), through Rh(-1.677 eV) to the right side case of Ag (-4.186 eV). Such an exception

may be due to the s^1d^9 valence electronic configuration in generating the potential adopted, rather than its ground state d^{10} configuration with fully filled *d* orbital in experiment, artificially shifting up the E_d of Pd. Importantly, the calculated E_d of the earlier TM, *i.e.*, Tc and Ru, are higher than that of pure Rh, whereas the later ones, such as Ag, possess lower E_d than that of pure Rh. Correspondingly, the interaction of the solute atoms with the surface Rh can be elucidated within the framework of a coupling between two single localized *d* orbitals with the energy levels of E_d(TM) and E_d(Rh), respectively. As schematically shown in Fig. 4, in the cases of Tc(Ru)@Rh(111), the coupling (hybridization) of these two orbitals definitely further lowers the E_d state of the host Rh (E_d(Host)) (as indicated by the position of host-dominated bonding state), because the solute atoms have relatively higher E_d, *i.e.*, E_d(Solute), see Fig. 4(a); on the other hand, for the cases of Pd(Ag)@Rh(111), the coupling of the solute orbital with relatively lower E_d(Solute) state with that of the host will further lift up the E_d(Host) (as indicated by the positon of the host-dominated anti-bonding state). Hence, in the TM@Rh(111) SSAs, the first layer host Rh atoms possess lower E_d in the cases of earlier TM solute atoms (Tc and Ru), as compared to that of the later ones, such as Pd and Ag, see also Figs. 3 and 4(b).

Now that we have established the underlying mechanism of the SSA effect in both the energetic and kinetic properties of carbon dimerization in the very early stages of graphene epitaxial growth on metal surfaces, we now continue to discuss the SSA effect on the energetics of relatively larger C clusters on metal substrates. Considering the diffusion and dissociation barriers of the C seeds, experimentally, there are still some possibilities in forming C clusters on the flat terraces of metal substrates on which graphene nucleation is energetically unfavoured. Hence, we also optimize the most stable configurations of C_N clusters (N=3~10) on all the investigated

TM@Rh(111) substrates (TM=Tc, Ru, Rh, Pd, and Ag). In searching for the most stable structures of C_N clusters, we consider both one-dimensional (1D) linear chains and 2D compact configurations. Our results show that in the studied size regime, C_N clusters prefer 1D chains on all the TM@Rh(111) substrates, see Fig. 5, in close agreement with previous findings.[47]

In Fig. 6(a), we present the average E_f per C atom of the C_N species (N=1~10) on the studied substrates, and in Fig. 6(b) the second-order differences of the E_f (Δ^2E_f) are presented. Significantly, both the binding energies and the stabilities of the C_N clusters on Rh(111) substrate can be modulated by the SSA effect. More specifically, the signs and/or the amplitude of the Δ^2E_f can be tuned to change from the case of pure Rh(111) via the introduction of the solute alloy atoms. For examples, as mentioned previously, C dimerization is energetically not preferred on pure Rh(111), therefore to stabilize the active C_2 dimer, a relatively large E_f is obtained, which is manifested by a negative Δ^2E_f at N=2. Whereas it is now changed to be positive on Tc(Ru)@Rh(111) substrates, confirming the preference of the C dimerization. Furthermore, at the size of N=3, significantly, C clusters are becoming more and more stable in a sequence of Tc@Rh(111)<Ru@Rh(111)<Rh(111)<Pd@Rh(111)<Ag@Rh(111), as supported by the gradually outstanding peak of the Δ^2E_f curves. Such phenomena are also observed in the even larger sizes regime (N=4~9), cofirming that the SSA effect in tuning the relative stabilites of the C seeds or C nucleas on metals. Note that, recently, DFT calculatons combined with experimental observations identified the magic number of N=21 for carbon clusters on Rh(111), Ru(0001), Ni(111), and Cu(111).[49] Consequently, it is very interesting to examine whether the SSA effect can change the magic number of the deposited C clusters in such a size regime on these substrates in our future work.

We now address the validity of the SSA effect in suppressing the orientation disordering of the graphene domains on the metal substrates. To do this, taking C_6 ring as a prototypical (actually the smallest) hexagonal compact graphene domain sample, we investigated its energetics between different orientations on the studied TM@Rh(111) substrates. Here, we consider two high-symmetry orientations (HSO): in the first case, the C_6 ring adsorbs flat on Rh(111) with its edge C atoms locating at the bridge sites between two surface Rh atoms (briefly, we name it HSO-B); and in the second, the six edge C atoms locate at the three-fold hollow sites of the surface Rh atoms (*i.e.*, HSO-H). As disucssed, a single C atom prefers to adsorb on the three-fold hollow site, rather than on the bridge site. Surprisingly, on both pure Rh(111) and TM@Rh(111) substrates, the smallest graphene domain (C_6) prefers the HSO-B configuration, namely, all the six C atoms locate on the bridge sites. Detailed analysis reveals that such unexpected results may be due to the geometric effect of the C_6 on hexagonal close-packed metal substrate. In the case of Rh(111), in the HSO-H configuration, the six C-C bonds cross the surface Rh-Rh bonds, which is energetically undesirable due to the C-C bending when the C atoms approach to the surface, resulting in larger average C-Rh bond length (2.24 Å) as compared to the 2.07 Å in the HSO-B orientation. Interestingly, the energy differences (ΔE=E(HSO-H)-E(HSO-B)) between these two orientations can be modulated by the SSA effect, as presented in Fig. 7. On the pure Rh(111) surface, the calculated ΔE is 2.214 eV; however, when the TM solute elements are to the left side of the host Rh, such as Ru and Tc, the values of the ΔE decrease to 1.783 and 1.684 eV, respectivly, energetically enhancing the trend of orientation disordering. On the other hand, when the TM solute elements are to the right side of the host Rh, for instance of Pd, the calcualted ΔE increases to 2.413 eV. Particularly, in the case of Ag@Rh(111), the HSO-H orientaiton is already not a local

energy minimum configuration with even higher energy, as schematically shown in the unfilled bar in Fig. 7. Natually, important message can be obtained from Fig. 7 on how to energetically suppress the orientation disordering of the graphene domains on a given host transition meal substrate, particularly those (such as Cu[24-27, 32]) on which multi-site nucleation is preferred: by the introduction of later solute TM atoms essentially with lower *d*-band centers in the SSA.

To the end, to verify the above hypothesis, we perform preliminary calculations on controlling the initial stage of C nucleation and suppressing the orientation disordering of graphene domains on Cu(111), which has been widely regarded as the most promising catalytic substrates for potential mass production of high-quality graphene via CVD method.[25, 26] Here, Zn is selected to serve as the solute elements in the SSA: the calculated E_d of Cu(111) and Zn(0001) are -2.195 and -6.684 eV, respectively, *i.e.*, the later possesses significantly lower *d*-band center than the former. Briefly, we first calculated the parameter of $\Delta E=E_{C\text{-}dimerization}-E_{C\text{-}separation}$ for two C adatoms on both pure Cu(111) and the Zn@Cu(111) SSA substrates. As presented in Fig. 8(a), on pure Cu(111), ΔE= -3.626 eV, indicating the preference of C dimerization, however, on the Zn@Cu(111) SSA substrate, the calculated ΔE is reduced to -3.157 eV. These findings demonstrate that, to some extent, the SSA effect may effectively tune the C nucleation process from a pure energetics perspective. Again, taking C_6 ring as a prototypical example, we then calculate the energy difference of two high symmetry orientation orderings (ΔE=E(HSO-H)-E(HSO-B)) of the graphene domain on Cu(111) and Zn@Cu(111) substrates. As shown in Fig. 8(b), on pure Cu(111), ΔE=0.022 eV, such a small energy difference elucidates again the origin of orientation disordering of graphene domains on Cu.[34, 52] However, on the Zn@Cu(111) SSA substrate, the calculated ΔE is shifted to -0.266 eV, and the negative sign

represents a reverse of the relative stabilities of these two HSOs, which may be due to the extra binding of C_6 ring with the sub-surface Zn atoms. Furthermore, we have also calculated the rotation barriers (E_{barr}) of the C_6 ring from the most stable orientation, *i.e.*, HSO-B (HSO-H) on Cu(111)(Zn@Cu(111)), to another low energy orientation, HSO-H (HSO-B), as inddicated by the arrowed lines, respectively, to check the SSA effect in tunning the rotational kinetics of graphenen domains on Cu(111). Our calculations show that on Cu(111), the C_6 ring seems to readily rotate due to the negligible barrier of 0.064 eV. However, on Zn@Cu(111) substrate, the SSA has greatly enhanced the rotational barrier up to 0.306 eV, see Fig, 8(c), kinetically suppressing its orientation disorder. Unambiguously, the significantly increased absolute values of both ΔE and E_{barr} have established the validity of the SSA effect in suppressing the orientation disordering of the graphenen domains[34, 52] and in optimizing the Cu substrate[24-27] for high quality graphene growth as well.

4. Conclusions

In conclusion, using first-principles calculations, we establish that sub-surface alloying effect can effectively modulate both the energetics and kinetics of carbon nucleation in the initial stages of graphene epitaxial growth on the metal substrate surface. Counter-intuitively, we reveal that the earlier TM solute atoms with higher *d*-band centers in the SSA can significantly enhance the C-dimerization and thus graphene nucleation on the host metal substrate. However, the later TM solute atoms with relatively lower *d*-band centers in the SSA may suppress both the graphene nucleation and the orientation disordering of the graphene domains. Such an interesting and simple picture can be well addressed in the framework of a delicate competition between C-C and

C-metal bonding modulated by the SSA effect, essentially obeying the *d*-band model. The present theoretical study reveals a highly predictive power of SSA tuning in the selection/design of appropriate substrate for mass production of single crystalline monolayer graphene in CVD experiment, as confirmed by our preliminary theoretical calculations on both Rh(111) and the widely used Cu(111) substrates. Therefore, we wish the present interesting results deserve of the development of elegant experimental technologies in fabrication of appropriate SSA substrates to examine the present theoretical findings for the practical applications in high quality graphene growth.

Acknowledgement

We thank Prof. Zhenyu Zhang for helpful discussions. This work was supported by the NSFC (Grants No. 11074223 and No. 11034006)

*z.x.guo@ucl.ac.uk
†sflizzu@zzu.edu.cn

References

1. K. S. Novoselov, A. K. Geim, S. V. Morozov, D. Jiang, Y. Zhang, S. V. Dubonos, I. V. Grigorieva and A. A. Firsov, *Science*, 2004, **306**, 666.
2. A. K. Geim and K. S. Novoselov, *Nat. Mater.*, 2007, **6**, 183.
3. A. H. Castro Neto, F. Guinea, N. M. R. Peres, K. S. Novoselov and A. K. Geim, *Rev. Mod. Phys.*, 2009, **81**, 109.
4. C. Lee, X. Wei, J. W. Kysar and J. Hone, *Science*, 2008, **321**, 385.
5. D. C. Elias, R. R. Nair, T. M. G. Mohiuddin, S. V. Morozov, P. Blake, M. P. Halsall, A. C. Ferrari, D. W. Boukhvalov, M. I. Katsnelson, A. K. Geim and K. S. Novoselov, *Science*, 2009, **323**, 610.
6. F. Bonaccorso, Z. Sun, T. Hasan and A. C. Ferrari, *Nat. Photon.*, 2010, **4**, 611.
7. M. Zhou, H. Bi, T. Q. Lin, X. J. Lu, F. Q. Huang and J. H. Lin, *J. Mater. Chem. A*, 2014, **2**, 2187.
8. C. Xiaomei, C. Zhixiong, C. Xi and M. Oyama, *J. Mater. Chem. A*, 2014, **2**, 5668.
9. C. B. Liu, H. Zhang, Y. H. Tang and S. L. Luo, *J. Mater. Chem. A*, 2014, **2**, 4580.
10. J. S. Zhou, J. M. Li, K. H. Liu, L. Lan, H. H. Song and X. H. Chen, *J. Mater. Chem. A*, 2014, **2**, 20706.
11. Y. Liu, X. Dong and P. Chen, *Chem. Soc. Rev.*, 2012, **41**, 2283.

12. C. Berger, Z. Song, X. Li, X. Wu, N. Brown, C. Naud, D. Mayou, T. Li, J. Hass, A. N. Marchenkov, E. H. Conrad, P. N. First and W. A. de Heer, *Science*, 2006, **312**, 1191.
13. K. V. Emtsev, A. Bostwick, K. Horn, J. Jobst, G. L. Kellogg, L. Ley, J. L. McChesney, T. Ohta, S. A. Reshanov, J. Rohrl, E. Rotenberg, A. K. Schmid, D. Waldmann, H. B. Weber and T. Seyller, *Nat. Mater.*, 2009, **8**, 203.
14. E. Starodub, S. Maier, I. Stass, N. C. Bartelt, P. J. Feibelman, M. Salmeron and K. F. McCarty, *Phys. Rev. B*, 2009, **80**, 235422.
15. S. Marchini, S. Günther and J. Wintterlin, *Phys. Rev. B*, 2007, **76**, 075429.
16. A. B. Preobrajenski, M. L. Ng, A. S. Vinogradov and N. Mårtensson, *Phys. Rev. B*, 2008, **78**, 073401.
17. P. Lacovig, M. Pozzo, D. Alfè, P. Vilmercati, A. Baraldi and S. Lizzit, *Phys. Rev. Lett.*, 2009, **103**, 166101.
18. J. N. D. Coraux, A. T.; Engler, M.; Busse, C.; Wall, D.; Buckanie, N.; Heringdorf, F.-J. M. z.; van Gastel, R.; Poelsema, B.; Michely, T, *New J. Phys.*, 2009, **11**, 023006.
19. Y. Zhang, L. Gomez, F. N. Ishikawa, A. Madaria, K. Ryu, C. Wang, A. Badmaev and C. Zhou, *J. Phys. Chem. Lett.*, 2010, **1**, 3101.
20. Y. Lee, S. Bae, H. Jang, S. Jang, S.-E. Zhu, S. H. Sim, Y. I. Song, B. H. Hong and J.-H. Ahn, *Nano Lett.*, 2010, **10**, 490.
21. P. Sutter, J. T. Sadowski and E. Sutter, *Phys. Rev. B*, 2009, **80**, 245411.
22. T. A. Land, T. Michely, R. J. Behm, J. C. Hemminger and G. Comsa, *Surf. Sci.*, 1992, **264**, 261.
23. S.-Y. Kwon, C. V. Ciobanu, V. Petrova, V. B. Shenoy, J. Bareño, V. Gambin, I. Petrov and S. Kodambaka, *Nano Lett.*, 2009, **9**, 3985.
24. L. Gao, J. R. Guest and N. P. Guisinger, *Nano Lett.*, 2010, **10**, 3512.
25. X. Li, W. Cai, J. An, S. Kim, J. Nah, D. Yang, R. Piner, A. Velamakanni, I. Jung, E. Tutuc, S. K. Banerjee, L. Colombo and R. S. Ruoff, *Science*, 2009, **324**, 1312.
26. Z. Sun, Z. Yan, J. Yao, E. Beitler, Y. Zhu and J. M. Tour, *Nature*, 2010, **468**, 549.
27. Z. Li, P. Wu, C. Wang, X. Fan, W. Zhang, X. Zhai, C. Zeng, Z. Li, J. Yang and J. Hou, *ACS Nano*, 2011, **5**, 3385.
28. Y. Cui, Q. Fu, H. Zhang and X. Bao, *Chem. Commun.*, 2011, **47**, 1470.
29. E. Loginova, N. C. Bartelt, P. J. Feibelman and K. F. McCarty, *New J. Phys.*, 2009, **11**, 063046.
30. E. Loginova, N. C. Bartelt, P. J. Feibelman and K. F. McCarty, *New J. Phys.*, 2008, **10**, 093026.
31. K. F. McCarty, P. J. Feibelman, E. Loginova and N. C. Bartelt, *Carbon*, 2009, **47**, 1806.
32. H. Chen, W. Zhu and Z. Zhang, *Phys. Rev. Lett.*, 2010, **104**, 186101.
33. W. Chen, H. Chen, H. Lan, P. Cui, T. P. Schulze, W. Zhu and Z. Zhang, *Phys. Rev. Lett.*, 2012, **109**, 265507.
34. P. Y. Huang, C. S. Ruiz-Vargas, A. M. van der Zande, W. S. Whitney, M. P. Levendorf, J. W. Kevek, S. Garg, J. S. Alden, C. J. Hustedt, Y. Zhu, J. Park, P. L. McEuen and D. A. Muller, *Nature*, 2011, **469**, 389.
35. G. Bihlmayer, P. Kurz and S. Blügel, *Phys. Rev. B*, 2000, **62**, 4726.
36. J. Schneider, A. Rosenhahn and K. Wandelt, *Appl. Surf. Sci.*, 1999, **142**, 68.
37. J.-H. Lee, E. K. Lee, W.-J. Joo, Y. Jang, B.-S. Kim, J. Y. Lim, S.-H. Choi, S. J. Ahn, J. R. Ahn, M.-H. Park, C.-W. Yang, B. L. Choi, S.-W. Hwang and D. Whang, *Science*, 2014, **344**, 286.
38. J. Greeley and M. Mavrikakis, *Nat. Mater.*, 2004, **3**, 810.
39. N. M. Markovic and P. N. Ross, *Surf. Sci. Rep.*, 2002, **45**, 121.

40. J. L. Zhang, M. B. Vukmirovic, K. Sasaki, A. U. Nilekar, M. Mavrikakis and R. R. Adzic, *J. Am. Chem. Soc.*, 2005, **127**, 12480.
41. B. Hammer, Y. Morikawa and J. K. Nørskov, *Phys. Rev. Lett.*, 1996, **76**, 2141.
42. A. Nilsson, L. G. M. Pettersson and J. K. Nørskov, *Chemical Bonding at Surfaces and Interfaces* (Elsevier, Amsterdam, 2008).
43. G. Kresse and J. Furthmüller, *Phys. Rev. B*, 1996, **54**, 11169.
44. P. E. Blöchl, *Phys. Rev. B*, 1994, **50**, 17953.
45. G. Kresse and D. Joubert, *Phys. Rev. B*, 1999, **59**, 1758.
46. J. P. Perdew, K. Burke and M. Ernzerhof, *Phys. Rev. Lett.*, 1996, **77**, 3865.
47. R. G. Van Wesep, H. Chen, W. Zhu and Z. Zhang, *J. Chem. Phys.*, 2011, **134**, 171105.
48. G. Henkelman, B. P. Uberuaga and H. Jónsson, *J. Chem. Phys.*, 2000, **113**, 9901.
49. Q. Yuan, J. Gao, H. Shu, J. Zhao, X. Chen and F. Ding, *J. Am. Chem. Soc.*, 2012, **134**, 2970.
50. H. Duan, N. Yan, R. Yu, C.-R. Chang, G. Zhou, H.-S. Hu, H. Rong, Z. Niu, J. Mao, H. Asakura, T. Tanaka, P. J. Dyson, J. Li and Y. Li, *Nat. Commun.*, 2014, **5**, 3093.
51. R. Ferrando, J. Jellinek and R. L. Johnston, *Chem. Rev.*, 2008, **108**, 845.
52. K. Kim, Z. Lee, W. Regan, C. Kisielowski, M. F. Crommie and A. Zettl, *ACS Nano*, 2011, **5**, 2142.

Figures:

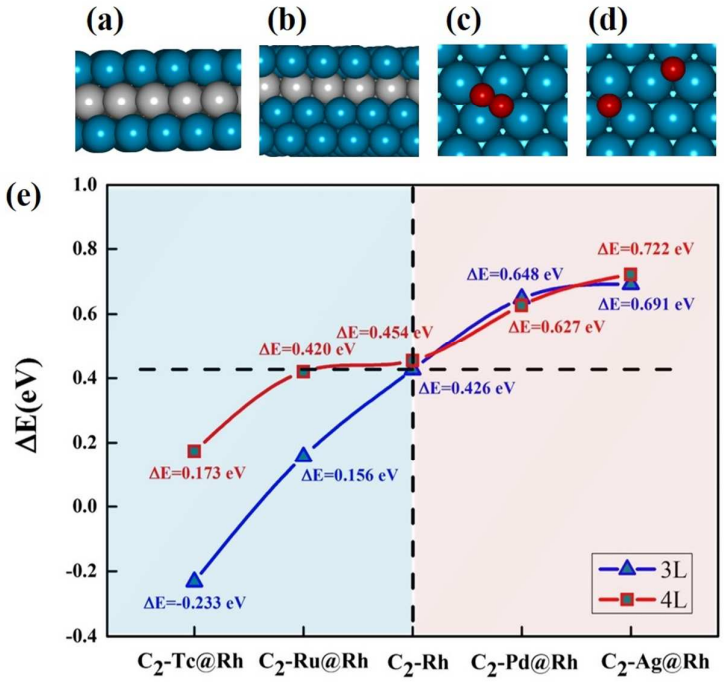

(Fig. 1, Zhang, *et al.*, to PCCP)

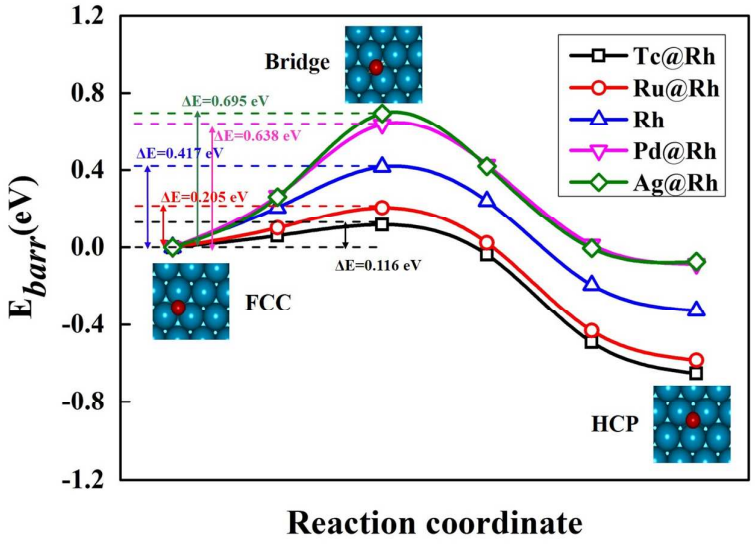

(Fig. 2, Zhang, *et al.*, to PCCP)

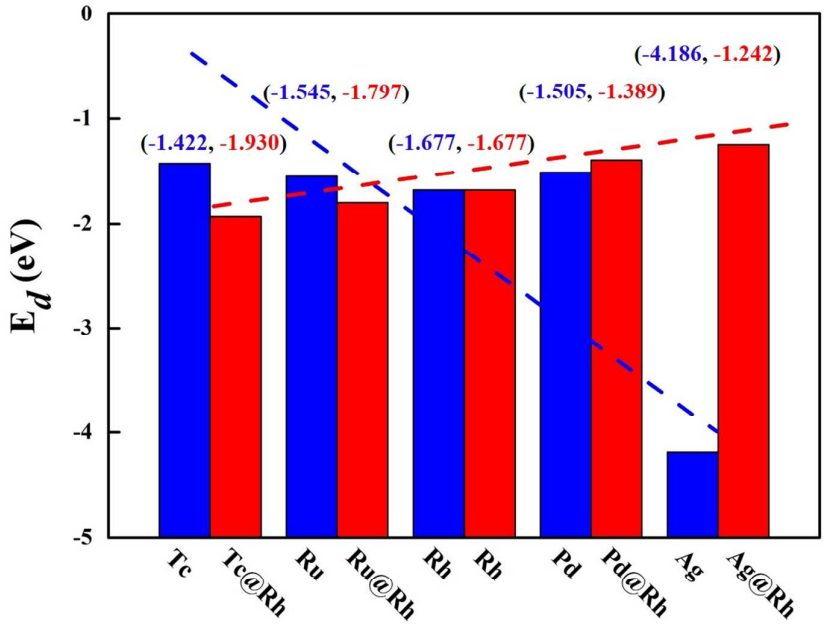

(Fig. 3, Zhang, *et al.*, to PCCP)

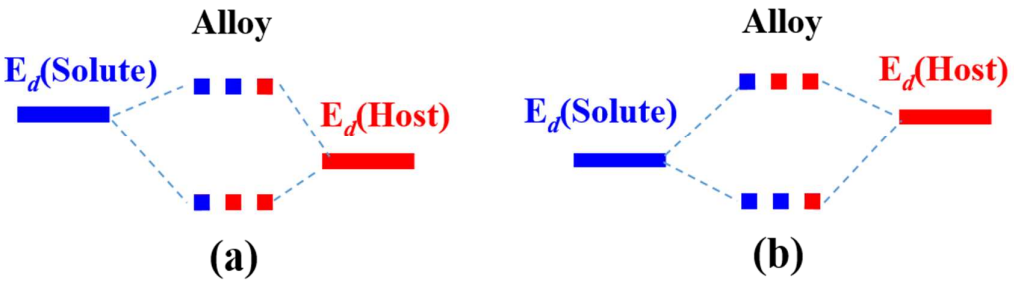

(Fig. 4, Zhang, *et al.*, to PCCP)

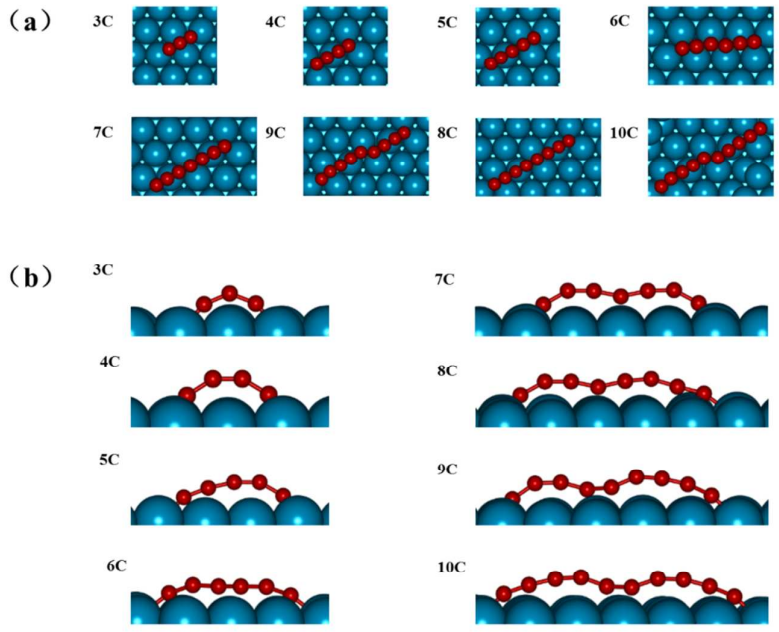

(Fig. 5, Zhang, *et al.*, to PCCP)

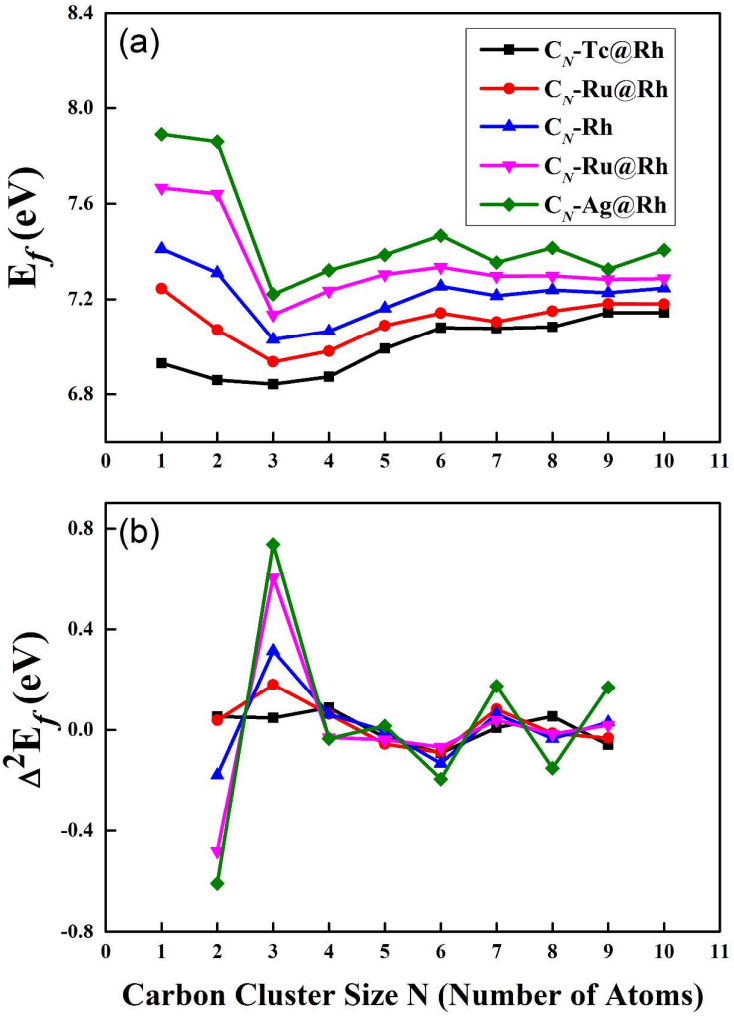

(Fig. 6, Zhang, *et al.*, to PCCP)

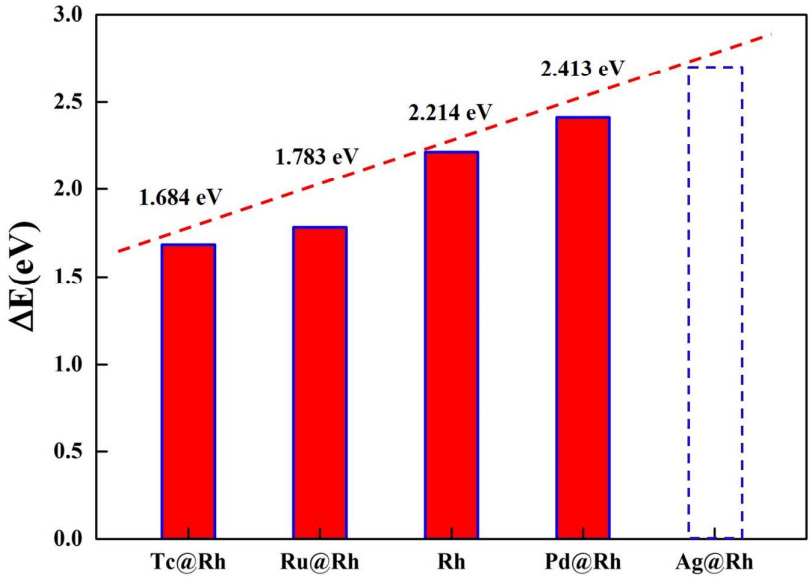

(Fig.7, Zhang, *et al.*, to PCCP)

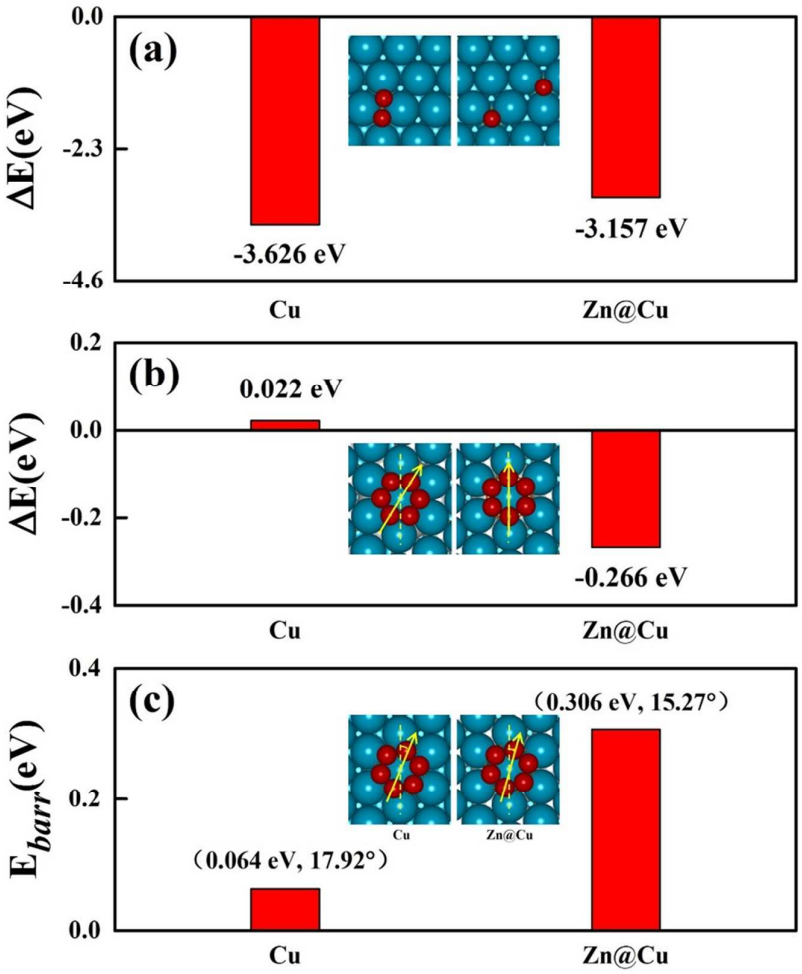

(Fig. 8, Zhang, *et al.*, to PCCP)

Figure Captions:

Fig. 1: (a) Three-layered sub-surface alloy (SSA) model (side view) with the solute transition metal intercalated between the first and the second layers; (b) four-layered slab model; (c) dimerization of two C adatoms on the SSA (top view); (d) two C adatoms with largest distance on the Rh(111) and SSA substrates; and (e) the energy difference (ΔE) between structures presented in (c) and (d), i.e., $\Delta E=E_{C\text{-}dimerization}-E_{C\text{-}separation}$. The data represented by triangles are calculated with the three-layered slab model (a), while the squares represent the data from the four-layered model (b).

Fig. 2: Minimum energy paths and energy barriers (E_{barr}) for a single C atom diffusion on Rh(111) and TM@Rh(111) SSA substrates from the fcc site to a nearby hcp site; the saddle points are nearby bridge sites.

Fig. 3: The *d*-band centers (E_d) of the top-most surface Rh atoms in pure Rh(111) substrate, TM@Rh(111) SSAs (TM=Tc, Ru, Pd, and Ag). For comparison, the E_d of the top-most surface TM atoms in Tc(0001), Ru(0001), Pd(111) and Ag(111) are also presented. All the E_d are calculated using a three-layered slab model.

Fig. 4: Schematic diagrams for the role of the interactions of the solute TM atoms with the host surface atoms in shifting their *d*-band centers.

Fig. 5: Optimized configurations of C_N clusters (N=3~10) on Rh(111); similar structures are obtained for C_N clusters on TM@Rh(111) SSA substrates.

Fig. 6: (a) Formation energy of C_N clusters, $E_f=(N\times E_{C(atom)}+E_{substrate}-E_{adsorbate\text{-}substrate})/N$, on Rh(111) and TM@Rh(111) SSA metal substrates; and (b) its second-order difference, $\Delta^2E_f=E_f(N+1)-E_f(N-1)-2E_f(N)$ for different C_N clusters.

Fig. 7: Energy differences between two optimized high symmetry orientations (HSO-B and

HSO-H) for C_6 ring on Rh(111) and TM@Rh(111) SSA substrates, ΔE=E(HSO-H)-E(HSO-B). For the case of Ag@Rh(111), the HSO-H orientation is not a stable configuration with much higher energy, which is only schematically shown by the unfilled bar.

Fig. 8: (a) Energy differences, $\Delta E=E_{C\text{-}dimerization}-E_{C\text{-}separation}$, for two C adatoms on both pure Cu(111) and the Zn@Cu(111) SSA substrates; **(b)** Energy differences between two optimized high symmetry orientations (HSO-H and HSO-B) for C_6 ring on Cu(111) and Zn@Cu(111) SSA substrates, ΔE=E(HSO-H)-E(HSO-B); and **(c)** Rotation barrier of the C_6 ring from the most stable orientation to the low-lying one. The geometric structures of the saddle points are inserted. In the bracket, the rotational barrier E_{barr} and the angle（θ）between the highest symmetric axis of the C_6 ring (indicated by the arrowed line) and that of the metal surface (by the dotted line) are presented in the bracket in the form of (E_{barr},θ).

A table of contents entry:

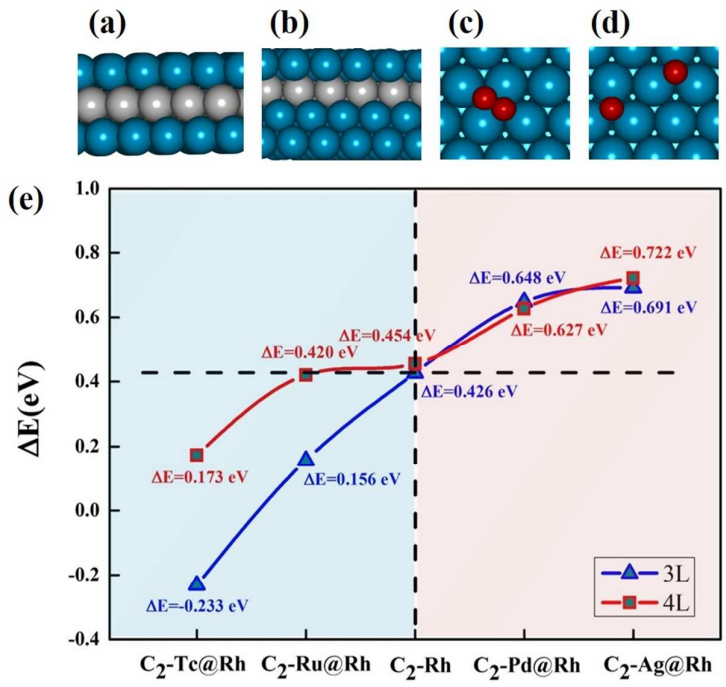

Sub-Surface Alloying Largely Influences Graphene Nucleation and Growth over Transition Metal Substrates